https://doi.org/10.5194/egusphere-2025-1961
Preprint. Discussion started: 19 May 2025


# Properties of large-amplitude kilometer-scale field-aligned currents at auroral latitudes, as derived from Swarm satellites

Yun-Liang Zhou[1*] and Hermann Lühr[2]

1. School of Earth and Space Science and Technology, Wuhan University, 430072 Wuhan, China

2. GFZ Helmholtz Centre for Geosciences, Section 2.3, Geomagnetism, Telegrafenberg, 14473 Potsdam, Germany

*Correspondence to: zhouyl@whu.edu.cn

**Abstract** High-resolution magnetic field recordings by the Swarm A and C spacecraft have been used to investigate the properties of field-aligned currents (FACs) at auroral latitudes down to their smallest scales (<1 km). Particularly suitable for that purpose are the magnetic field recordings, taken at a rate of 50 Hz, during the two weeks around the quasi-coplanar orbit configuration on 1 October 2021. We have split the recorded signal caused by FACs of along-track wavelengths from 0.3 km to 40 km into 8 quasi-logarithmically spaced ranges. Our investigations revealed that the kilometer-scale FACs (0.3- 5 km) show quite different characteristics from those of the small-scale FACs (10-40 km). The kilometer-scale FACs exhibit short-lived (<1 s) randomly appearing large current spikes. They are confined to certain latitude ranges, which depend on local time. Small-scale FAC structures last for longer times (>10 s) and are distributed over larger latitude ranges. Their largest amplitudes are achieved at latitudes that overlap with the kilometer-scale FACs. The small-scale FACs have earlier been identified as Alfvén waves that are partly reflected at the ionosphere, and they can oscillate within the ionospheric Alfvén resonator. When at the same time additional Alfvén waves are launched from the magnetosphere they will interfere with the reflected. We suggest that the interaction between oppositely travelling Alfvén waves, when continuing sufficiently long, is generating the large-amplitude and short-lived kilometer-scale FACs.

## 1. Introduction

Field-aligned currents (FAC) in the ionosphere are a commonly observed phenomenon. In particular, at auroral latitudes they act as coupling agents between plasma processes in the magnetosphere and the ionosphere. ~~There are various types of~~ FACs ~~coming with~~ horizontal scales in the ionosphere from about 1 km (e.g., Neubert and Christiansen, 2003; Rother et al., 2007) up to some1000 km (e.g., Iijima and Potemra, 1976; Anderson et al., 2014). In general, the current densities become larger the smaller the scale of the FAC. In most cases, pairs of upward and downward currents appear close together. Thus, small-scale FACs, with their high density, contribute only little to the net current between magnetosphere and ionosphere, but they can transfer a significant amount of energy into the ionospheres (e.g., Lühr et al., 2004).

Multi-spacecraft missions have been used to evaluate the properties of FACs with different sizes. For example, Gjerloev et al. (2011) made use of the three ST5 satellites in pearls-on-a-string formation. By comparing the magnetic field readings of successive spacecraft, they found that FACs with scales larger than 100 km on the nightside can be considered as stationary (for at least 1 min), while on the dayside this was only valid ~~for~~ scale above 200 km. With the help of the three Swarm satellites Lühr et al. (2015) ~~could~~ confirm these findings~~, but they~~ extended the analysis to smaller scales down to some 10 km. Those ~~current features showed a lot of~~ temporal variability at periods of about 10 s~~. They can no longer~~ be treated as stationary structures. At those scales magnetic field lines cannot be regarded any longer as equipotential lines.

In a recent study, Lühr and Zhou (2025) extended the FAC scale analysis at auroral latitudes by making use of the Swarm Counter Counter-Rotating Orbit Phase in 2021. During that campaign the orbits of Swarm A and C were brought close together, and Swarm B cycled the Earth in opposite direction. Around 1

https://doi.org/10.5194/egusphere-2025-1961
Preprint. Discussion started: 19 May 2025


October 2021 all three orbital planes were quasi-coplanar. Thereafter, the orbits slowly separated again. By means of a cross-correlation analysis it was checked how well the signals at the two spacecraft agree. Over the course of the study period the cross-track separation covered the range between 0 and 30 km at the equator-crossing point, and the along-track separation ~~was~~ varied from 2 s to 41 s. ~~Obtained~~ results confirm ~~largely~~ earlier findings. Current structures with apparent periods of more than 15 s (corresponding to ~~an~~ along-track wavelengths of >100 km) exhibit good correlations between the magnetic field signals at the two accompanying spacecraft for all experienced along- and cross-track separations. However, for apparent periods of less than 10 s (<75 km wavelength) the properties changed. Here significant correlations were only achieved when the cross-track separation was below about 6 km and the along-track separation below 18 s. These results indicate that FACs ~~of~~ these scales are no longer organized as current sheets but represent current filaments.

~~In spite of all these results about FAC properties,~~ not much is known about the characteristics of FACs ~~with horizontal scale-lengths of some kilometer (km-scale FACs). In dedicated studies, e.g.,~~ Neubert and Christiansen (2003); Rother et al. (2007) have shown ~~the large amplitudes,~~ these narrow FACs can attain. They appear on the dayside ~~preferably~~ at high auroral latitudes in the cusp region, around noon~~,~~ and in the prenoon sector. On the nightside, generally smaller amplitudes ~~have been observed,~~ and their appearance coincides ~~there~~ with the westward electrojet. No information is ~~provided so far~~ about their temporal and spatial correlation lengths.

~~For improving that situation,~~ this study ~~makes~~ use of the high-resolution 50 Hz magnetic field samples ~~of~~ the Swarm A and Swarm C satellites. These data provide sufficient resolution for investigating the details of the smallest FAC features. Particularly suitable for that purpose are the weeks around 1 October 2021, when Swarm A and C orbits were quasi coplanar and the along-track separation reduced to 2 s. This unique dataset will be used for determining the temporal and spatial correlation lengths of these smallest FAC features.

In the sections to follow we will first introduce the instruments and data considered here. In Section 3 some examples are presented showing typical features of the narrow FACs. For a better characterization of the FACs with various scales Section 4 presents a separation of the magnetic field signal into 8 period bands. Section 5 provides a statistical analysis of the FAC signals at different scales by means of the ellipticity properties. A discussion of the results and their relations to earlier publications is presented in Section 6. Finally, in Section 7 the important findings are summarized and conclusions are drawn.

## 2. Data and processing approach

ESA's Earth observation mission Swarm was launched on 22 November 2013. It consists of three identical satellites in near-polar orbits at different altitudes. During the first mission phase, starting on 17 April 2014, Swarm A and C were flying almost side-by-side, separated by1.4° in longitude, at an altitude of about 460 km and an inclination of 87.3°. Swarm B is orbiting the Earth about 60 km higher with an inclination of 88°. This difference in inclination causes a slowly increasing difference in longitude between the two orbital planes amounting to about 2° per month.

After almost 8 years in orbit a counter-rotating configuration was achieved between the Swarm A/C pair and Swarm B (for more details see Xiong and Lühr, 2023). Around 1 October 2021 the orbital planes of Swarm A/C and Swarm B crossed the equator at similar longitudes. During the two years before that date the longitudinal separation between Swarm A and C had been slowly decreased, such that orbital coplanarity of Swarm A/C was also achieved on 1 October 2021. Furthermore, the along-track separation between Swarm A and C was varied during the months around coplanarity (see Zhou et al. (2024), Fig. 1). Here we focus on the weeks when the along-track separation was reduced to 2 s.

Each of the three satellites is equipped with a set of six instruments (Friis-Christensen et al., 2008). In this study, we use the data from the Swarm Vector Field Magnetometer (VFM). This fluxgate magnetometer is

https://doi.org/10.5194/egusphere-2025-1961
Preprint. Discussion started: 19 May 2025


sampling the field vector at a rate of 50 Hz. For maintaining high data precision over the years, the VFM data are calibrated routinely against the readings of the Absolute Scalar Magnetometer (ASM).

Basis for this study are the Swarm Level-1b 50 Hz magnetic field data with the product identifier "MAGx_HR", where the lower-case "x" in the product names is a placeholder for the spacecraft names, A, B, or C. The magnetic vector data are given in the North-East-Center (NEC) frame. Of interest here are the magnetic signatures caused by FACs at auroral latitudes. For isolating these signatures from other magnetic field contributions, the geomagnetic field model CHAOS-7.18 (Finlay et al., 2020) is subtracted from the full-field readings. This model represents the contributions of Earth core and crustal fields and the effects of large-scale magnetospheric current systems. Since we are interested in the smallest scales of FAC structures, the data are in addition high-pass filtered with a cutoff frequency of about 0.2 Hz. This removes small biases of the CHAOS model and suppresses the longer-period contributions from E-region current systems like the auroral electrojets or the polar cap return currents.

The bandlimited residuals of the horizontal components, *Bx* and *By*, are used for studying the magnetic signatures caused by the FACs. From these two components we calculate the deflections of, $B_{trans}$, transverse to the flight direction and $B_{along}$, aligned with the flight direction. They are derived by the transformation

$$B_{trans} = B_y \cos(\gamma) - B_x \sin(\gamma) \quad (1)$$
$$B_{along} = B_x\, cos(\gamma) + B_y\, sin(\gamma)$$

where $sin(\gamma) = cos(incl)/cos(lat)$ with *incl* as orbital inclination and *lat* as latitude of the measurement point. For application in Eq. (1) $\gamma = \gamma$ has to be used on the ascending part of the orbit and $\gamma = \pi - \gamma$ on the descending part. These horizontal components, $B_{trans}$ and $B_{along}$, are sufficient for studying the FAC properties since the field lines are almost vertical at auroral latitudes.

## 3. Representative examples

In an earlier study, Lühr and Zhou (2025) made ~~already~~ use of the close spacing between the Swarm A and C satellites during the counter-rotating orbit phase. By means of a cross-correlation analysis the correlation length both in space and time could be determined for small- and meso-scale FAC structures. These authors found, as expected, a progressively decreasing persistence in space and time towards smaller current structures. Since we are focusing here on the very small FACs, we tried the same cross-correlation approach with data when the spacecraft were closest together. This occurred during the 16 days, 18 September - 4 October 2021.

Figure 1 presents two example orbits from northern hemisphere auroral region crossings on 21 September 2021. Shown are in the top panel of the frames a direct comparisons between the magnetic recordings by Swarm A and C. Here the $B_{trans}$ component is used. This component, perpendicular to the orbit track, shows clearest the variations of the FACs. Furthermore, its time derivative is displayed since it is directly proportional to the FAC density estimates, as outlined by Lühr and Zhou (2025). A $\Delta B_{trans}$ = 10 nT/s corresponds to 1.1 μA/m$^2$ when assuming a perpendicular crossing of a plane FAC sheet. The second panel shows the RMS values of $\Delta B_{trans}$ derived over a 16 s period. In the third panel the lag time, T-lag, for an optimal cross-correlation coefficient is given. Interestingly, the obtained T-lag values stay, over large parts of the orbital arc, close to the actual along-track spacecraft separations, Δt = 2.1 s (listed in the header of the frames). Conversely, the peak cross-correlation coefficient, *Cc* (bottom panel), is generally quite low, well below our threshold of 0.75. Across the bottom of the frames, we have listed information along the orbit of Swarm A. Besides the time there are magnetic latitude (MLat), magnetic local time (MLT), and the cross-track distance, $d_{cross}$ in km, between Swarm A and C.

https://doi.org/10.5194/egusphere-2025-1961
Preprint. Discussion started: 19 May 2025


During both orbits, bursts of intense fine-scale features are observed with amplitudes surpassing partly1000 nT/s (corresponding to 100 μA/m$^2$). They occurred predominantly in the morning and prenoon sector but also on the nightside, here less intense. It is obvious to see that the coefficient, *Cc*, goes down in the regions of the bursts. This may be surprising since the cross-track spacecraft separation is only 1 km on the dayside and 2 km on the nightside. The question that arises here is, what causes the difference between the signals at Swarm A and Swarm C? Is it the spatial cross-track distance or the along-track time difference of 2.1 s? Answering this question will be part of the study.

In order to get a better understanding of the small FAC characteristics, Figure 2 shows for two bursts of activity a zoom into the magnetic signatures recorded by the two horizontal components, $\Delta B_{trans}$ and $\Delta B_{along}$. Presented are intervals of 15 s, corresponding to about 100 km along-track. In the top frame observations from the late morning sector are plotted. Here, the recordings by the two spacecraft have little in common although the time-shift, $\Delta t$ = 2.1 s, between them has been accounted for. The lower frame is from the nightside. Also here, the signal at the two spacecraft differ significantly during active periods. Still, for longer-period variations, of order 5 s and longer, the curves seem to follow each other reasonably well. From these observations we may conclude, the longer period signals are responsible for the optimal time shift derived by the cross-correlation in Figure 1, fitting the actual along-track separation of $\Delta t$ = 2.1 s. On the other hand, the higher-frequency fluctuations are causing the low *Cc* values, even at optimal time shift. Also, when visually comparing the $\Delta B_{trans}$ and $\Delta B_{along}$ signals in Figure 2, hardly any correlation between the two components can be found. This indicates that the shape of the FAC filaments is constantly changing.

The magnetic signature within the bursts covers a wide frequency spectrum. There is no clear preference for any frequency. Even very narrow features in $\Delta B_{trans}$, e.g. around 23:09:48 UT and 16:47:55 UT, can reach large amplitudes. More details of the signal spectrum will be provided in Section 5.2. The FAC burst events in the upper and lower frames of Figure 2 are from the day and night sides, respectively. Therefore, they are connected to very different source regions in the magnetosphere, but still, their characteristics are very similar. A pending question here is, what causes the fragmentation into the small filaments. By looking into a larger number of events we may find systematic characteristics.

## 4. Separation of the signal into period bands

From the examples presented above it is obvious that the FAC-related magnetic signal within the bursts covers a wide frequency range, and the variations of $\Delta B_{trans}$ and $\Delta B_{along}$ are quite independent from each other. Figure 2 furthermore suggests that the correlation properties between Swarm A and C vary with the apparent period (along-track scale length) of the signal. In order to identify the typical FAC properties we investigated the signal of the whole study period, 18 September to 4 October 2021, the days when the along-track separation was reduced to 2 s. Furthermore, we subdivide the signals of $\Delta B_{trans}$ and $\Delta B_{along}$ into eight quasi-logarithmically spaced period bands. The chosen -3 dB pass-band filter limits are 0.04-0.1 s, 0.1-0.16 s, 0.16-0.26 s, 0.26-0.44 s, 0.44-0.72 s, 0.72-1.2 s, 1.2-2.5s, and 2.5-5 s. The last two period bands overlap with the spectral range of the FAC study by Lühr and Zhou (2025). In this way we want to extend that earlier study and find the relation between the km-scale and small-scale FAC characteristics. The apparent signal periods recorded by the satellites represent an along-track wavelength of the current structure. Following the arguments of the earlier study we also here define halve the wavelength as the scale size of a FAC.

We have performed a cross-correlation analysis between the $\Delta B_{trans}$ components of the two satellites separately for the above listed period bands. A number of criteria are defined for separating quasi-stationary FAC features from uncorrelated signal parts. The peak cross-correlation coefficient should be *Cc* > 0.75 at a time shift close to the spacecraft separation time, $\Delta t$, thus has to be *T-lag* = $\Delta t \pm 1.5$ s. In order to make sure that only intense auroral FACs are considered, the signal variation, $\Delta B_{trans}$, should surmount an amplitude threshold, RMS > 2 nT/s. An equivalent set of criteria has been used by Lühr and Zhou (2025);

https://doi.org/10.5194/egusphere-2025-1961
Preprint. Discussion started: 19 May 2025


therefore, direct comparisons between the two studies are possible. The detailed parameters for the cross-correlations are listed in Table 1.

Table 1: Listing of the data interval lengths and step sizes for the cross-correlation analysis of the various period bands.

| Period band | Data interval | Step size |
|---|---|---|
| 0.44-0.72 s | 2 s | 0.24 s |
| 0.72-1.2s | 4 s | 0.5 s |
| 1.2-2.5 s | 8 s | 1 s |
| 2.5-5 s | 16 s | 2 s |

Figure 3 presents from the northern (top) and southern (bottom) hemispheres a series of cross-correlation results for the four longest period bands, over the study period. Shown is the latitude distribution of the fractions of correlated events compared to all events that exceeding RMS = 2 nT/s, separately for each orbit. White patches appear where no entries are available. Across the bottom of the frames we have listed the dates, magnetic local time (MLT) at 70° MLat, the along-track time difference, Δt, and the longitude separation between Swarm A and C at the equator. There are different frames for up- and downleg orbital arcs, obtained from local time sectors separated by about 12 hr. Displayed are the ratios from the signal bands covering the apparent period range from 0.44 s to 5 s (1.7-19 km scales).

All four frames in Figure 3 show an obvious change in correlation characteristic between the longest band (top panels) and the shorter periods. A large majority (80% - 100%) of the magnetic signatures in the 2.5 s -5 s period band (10-20 km scale) is well correlated between the two Swarm satellites. The smaller scale current structures show much lower percentages of correlated features. Some exceptions are observed at the lower latitude end around 65° MLat, particularly on the dayside. This is especially true for the northern hemisphere and to a lesser extend to the nightside. For all the other regions and the shorter periods, the ratio of well-correlated events is low, typically below 20%.

Here we like to recall the small separation between Swarm A and C, e.g. the 2 s time difference in along-track and a 0.5 - 2.5 km separation in cross-track direction during the two weeks of interest. The smallest cross-track separations occurred in the northern hemisphere at late morning hours and lower auroral latitudes (see Fig. 1). This is probably one reason for the enhanced ratios in that time sector and hemisphere. Conversely, in the southern hemisphere the shortest cross-track separations occur in the late evening to night sector and the longest in the morning, prenoon sector. These facts contribute to the differences between the ratio distributions in the two hemispheres.

Quite outstanding are the high percentages of quasi-stationary FAC structures in the northern hemisphere for the longest period range, 2.5-5 s. This fact is valid for almost all latitudes except for a band between 75° and 80° MLat on the dayside and at somewhat lower latitudes on the nightside. The point of reduced correlation will be revisited in Sections 5.2 and 6. On the other hand, hardly any well-correlated observations are found between Swarm A and C for periods shorter than 1 s. This suggests, the FAC structures with along-track wavelength of less than 7.5 km have a very short life-time, less than the 2 s, the lag-time between the sampling of the two satellites. It implies that the two Swarm satellites, even during this special constellation phase, cannot be used for estimating the FAC density of these narrow scales by means of the dual-satellite method (Ritter et al., 2013; Lühr et al., 2020). However, for the signals with periods longer than 2.5 s (>10 km scale) it can be used.

## 5. Statistical analysis

https://doi.org/10.5194/egusphere-2025-1961
Preprint. Discussion started: 19 May 2025


### 5.1 Polarization characteristic of FAC-related B-fields

When estimating FAC density from satellite magnetic field measurements a number of assumptions have to be made. This is in particular true when single-spacecraft measurements are interpreted. Most reliable results can be achieved when plane FAC sheets are crossed. In those cases, the two horizontal field components vary in phase. Conversely, when the satellite passes outside of the sheet or when the FAC has a filamentary shape, there exists a significant phase shift between the magnetic signatures of the two components. In those cases, FAC density estimates are difficult.

In order to determine the magnetic signal properties, we analysed their ellipticity parameters from the data of the two horizontal components, $B_{trans}$ and $B_{along}$. For estimating the polarization parameters, we made use of the approach outlined by Fowler et al. (1967). In this way the following quantities are derived: the *Ratio* of polarized signal within the total signal, the degree of *Ellipticity* (a zero means linearly polarized, a +1 stands for right-handed circular and -1 for left-handed circular polarization), $\theta$ is the angle between the ellipse major axis and the $B_{trans}$ component, $f_{peak}$ reflects the frequency of the spectral peak within a given filter band, $Amp_{peak}$ shows the signal amplitude at $f_{peak}$ derived from the combined signal of the two components.

For the calculation of the ellipticity parameters we consider intervals of data that are twice as long as the longest period in a band and the step for successive processing is one quarter of the interval length. All these parameters are listed in Table 2 for the eight period bands. In this way we obtain a sufficiently detailed resolution of the signal variation at the various wavelengths. The basis for the ellipticity analysis is the Fourier transform of the magnetic field recordings. We have considered for the further analysis, from each period band, only the four lowest frequency Fourier coefficients in the band (ignoring the constant part) because the higher frequencies fall beyond the filter cut-offs of the band-passes and represent mainly leakage effects. Just for the two longest period bands (1.2-2.5 s and 2.5-5 s) the five lowest frequencies are taken into account because of their larger bandwidth.

Table 2: Listing of the data interval lengths and step sizes for the ellipticity analysis of the various period bands

| Period band | Scale size | Data interval | Step size |
|---|---|---|---|
| 0.04-0.1 s | 0.15-0.4 km | 0.2 s | 0.06 s |
| 0.1-0.16 s | 0.4-0.6 km | 0.32 s | 0.08 s |
| 0.16-0.26s | 0.6-1 km | 0.52 s | 0.13 s |
| 0.26-0.44 s | 1-1.7 km | 0.88 s | 0.22 s |
| 0.44-0.72 s | 1.7-2.7 km | 1.44 s | 0.36 s |
| 0.72-1.2s | 2.7-4.5 km | 2.4 s | 0.6 s |
| 1.2-2.5 s | 4.5-9.4 km | 5 s | 1.25 s |
| 2.5-5 s | 9.4-19 km | 10 s | 2.5 s |

Figure 4 presents a compilation of the various ellipticity parameters and shows examples of comparisons with the actual data. Representative for the other filter bands, here the 0.16-0.26 s period range is selected. The analysis is applied to the active 2-second interval recorded by Swarm A on 21 September 2021, 23:09:47 to 23:09:49 UT. The signal context surrounding this bursty period can be seen in Figure 6a. From the dynamic spectrogram in the top of Figure 4a the limiting effect of the applied bandpass is clearly visible. Time-line plots of the two magnetic components exhibit largest amplitudes around 23:09:48.3 UT, as is

https://doi.org/10.5194/egusphere-2025-1961
Preprint. Discussion started: 19 May 2025


also obvious from the spectrogram. In the frame below, the Ratio, in the bottom panel, stays close to 1, indicating that the magnetic recordings can well be interpreted in terms of ellipticity for most of the time. The value of Ellipticity ~~stays over two-third of the time close to zero~~, indicating a flat ellipse. Only during the first third of the interval a more developed ellipse is expected. These two regimes of Ellipticity exhibit also quite different angles between the ellipse major axes and the $B_{trans}$ direction. Over the first third of the ~~time~~, we find large $\theta$ angles, up to 90°, while during the remaining two-third small positive $\theta$ values dominate. The spectral peak varies between frequencies of 5 and 6 Hz, as expected for this filter band. The derived amplitude, $Amp_{peak}$ (modulus of the combined $B_{trans}$ and $B_{along}$) tracks well the signal intensity and reaches 20 nT around 23:09:48.3 UT.

The groups of panels in the lower part, Figures 4b and 4c, show details of the results, taken along the line of processing steps, obtained from times of the two contrasting ellipticity regimes. In Figure 4b, a time interval close to the signal maximum, the lower panels repeat the magnetic recordings of the two components. The dashed line represents the truncated spectrum and confirm that the four lowest frequencies, track the observation signals well. In the panels of the upper group, we find a nearly linearly polarized ellipse. Conversely, in the panels of Figure 4c, derived from the early-time conditions, a clear phase differences between the magnetic field components ~~can be found.~~ As a consequence, the hodograph shows a well-developed ellipse. All these derived ellipticity parameters will be used for estimating FAC densities at the various horizontal scales.

### *5.2 Deriving FAC density from ellipticity parameters*

From the examples of magnetic field recordings, shown in Figures 1 and 2, it is obvious that bursts of small-scale FACs with large amplitudes can be found both on the day and night sides. A question of interest is, are there preferred FAC scales sizes for the very large amplitudes? We thus tried to estimate the FAC densities separately for each period band. Due to the obvious filamentary shape of these small FACs there is no simple approach for obtaining reliable density values. Our chosen approach is thus to identify signatures of field variation that favor reliable FAC estimates.

The starting equation for commonly used FAC estimates from single-satellite magnetic field recordings is

$$j_z = \frac{1}{\mu_0}\frac{\Delta B}{v_{SC}} \quad (2)$$

where $\Delta B$ is the time derivative, $dB/dt$, of the vector formed by the components, $B_{trans}$ and $B_{along}$, $v_{SC}$ is the spacecraft velocity of 7.5 km/s, and $\mu_0$ is the permeability in vacuum. Here, the crossing of a plane FAC sheet at right angle is assumed. In general cases there exists an angle, $\theta$, between the sheet and the cross-track direction. Then the equation reads

$$j_z = \frac{1}{\mu_0}\frac{\Delta B}{v_{SC}\cos(\theta)} \quad (3)$$

For the application of this equation to our small-scale FACs we make use of the ellipticity parameters. For example, the maximum magnetic field change can be calculated from the derived peak amplitude and frequency

$$\Delta B_{peak} = 2\pi\, Amp_{peak}\, f_{peak} \quad (4)$$

Not all ~~the~~ recorded wavy signal are suitable for FAC estimates. Therefore, we introduced 4 conditions for considering only the clean ones. (i) For obtaining clear ellipticity we request Ratio > 0.7. (ii) Most reliable results are derived when the satellite crosses quasi-planar sheets of FACs indicated by near-linear polarization or a small Ellipticity value. We thus require, |Ellipticity| < 0.3. (iii) In order to avoid problems from crossing the current sheet at too shallow angles, we request $|\theta| < 60°$. (iv) Finally, too small signals, which may be caused by waves, are ignored by requiring, $\Delta B_{peak} > 3$ nT/s.

https://doi.org/10.5194/egusphere-2025-1961
Preprint. Discussion started: 19 May 2025


Figure 5a presents, as an example, for a 2-min interval of intense FAC activity (see Fig. 6a), the derived ellipticity parameters of the period band, 0.26-0.44 s. The five panels contain the derived values for the ellipticity parameters. Dashed horizontal lines in the panels mark the ~~above descried~~ thresholds. Starting from the bottom, the Ratio is for most of the times above the limiting level of 0.7. The Ellipticity, in the panel above, is ~~commonly~~ small, thus suitable for FAC estimates. Also, the angle $\theta$ stays mostly inside the allowed range. In a majority of cases the angle ~~can be found~~ in the positive range. This is consistent with a ~~preferred alignment of the~~ FAC sheet ~~close to the~~ geomagnetic latitude ~~circle.~~ As expected, the spectral peak varies about the central frequency, 3.5 Hz, of the period band. Finally, the signal closely tracks the signal activity shown in Figure 6a. The $\Delta B_{peak}$ (see scale on right side) is calculated from the peak amplitude and peak frequency (see Eq. (4)).

For comparison, Figure 5b shows the same set of ellipticity parameters but now for the longest period band, 2.5-5 s. The amplitude variations in the top panel track quite well the activity variations shown in Figure 5a for the shorter-period signals. Otherwise, there are obvious differences. For example, the Ratio is on average lower, staying over longer periods close to the threshold. This indicates the presence of inharmonic signal, not contributing to the ellipticity. The Ellipticity, in the panel above, attains in several cases of sufficient Ratios large values outside the allowed band. For the angle $\theta$ we obtain again predominately positive values. The spectral peak is found around 0.4 Hz (2.5 s period) at the upper boundary of the period band. Worth noting is the difference in $\Delta B_{peak}$, the scale range is smaller by a factor of 10 than that of the 0.26-0.44 s period band. This indicates a rapid decrease of FAC peak amplitudes towards larger structures.

With this information at hand, we can estimate the FAC density wherever the ellipticity parameters stay within the allowed ranges. Figure 6a presents the magnetic variations of the 2-min interval taken as an example. It is the same as considered in Figure 5. In Figure 6b we show the derived FAC densities for all the 8 period bands. Both the results from Swarm A and C are plotted. Since Swarm C sampled the same region 2 s later, its data series can be considered as independent from Swarm A. As can be seen in Figure 6b, the current estimates from the two spacecraft complete each other quite well for the period bands shorter than 1 s. Thus, for them a fairly complete coverage is achieved. Times of enhanced and reduced FAC activity can well be tracked through all periods.

Just the two longest periods exhibit fairly large gaps appear between valid FAC estimates. We have looked into the reasons for the gaps by checking the ellipticity parameters. Starting with the 2.5-5 s period band, in total 48 values are expected from Swarm A. From them 37 did not pass all the checks. Reasons were in 24 cases too large Ellipticity, in 20 cases too large angle $\theta$ and 17 times too small Ratio. As is obvious from the sum of these listed cases, two of the violations often occurred at the same time. Here a large Ellipticity was frequently accompanied by a large $\theta$. Similar reasons have been deduced for the gaps in FAC density curves of the 1.2-2.5 s period band. These results ~~infer~~ that field-aligned currents in the period range longer than one second (>5 km scales) are ~~preferably~~ organized in filaments rather than current sheets.

It is interesting to note that the FAC peak amplitudes vary with the period (scale size). When looking at the panels of Figure 6b, we find small current density values for the shortest period. The value increases rapidly towards the period band of 0.16-0.26 s. Largest FAC peak densities are observed in the 0.16 - 0.44 s period range (0.5 - 1.5 km scale size) reaching values up to 60 $\mu A/m^2$. For longer periods the amplitudes drop again. In the 2.5 - 5 s period band peak values are already down by about a factor of 5.

For verifying our FAC density estimates we performed a comparison with the densities derived by the basic single-satellite approach, as given in Eq. (2). For $\Delta B$ we made use of the $\Delta B_{trans}$ from the 1.2-2.5 s and 2.5-5 s period bands. The two panels of Figure 6c show RMS values of the FAC densities as continuous curves from Swarm A and C, derived by the classic approach. For comparison, the partly available FAC densities from our ellipticity approach are added as heavy line segments. In principle, similar values are achieved by the two methods. It is expected that the ones from ellipticity are larger because they report the peak amplitude while we have shown the RMS values from the basic approach. It is convincing to see that the

https://doi.org/10.5194/egusphere-2025-1961
Preprint. Discussion started: 19 May 2025


two very different techniques of FAC estimates provide quite similar results. Both methods confirm the reduction of FAC amplitudes towards longer periods (larger scales).

For supporting our suggestion of filamentary small-scale FAC structures we made some simple model calculations. As outlined by a cartoon on the left side of Figure 7, we assume a fluxtube with circular cross-section of radius, $r$ = 10 km. For four satellite tracks past the tube center at distances $e$ = 20, 7, 5, 1 km we calculate the $B_{trans}$ and $B_{along}$ variations when assuming a current strength $I$ = 1 kA and homogeneous current density distribution within the fluxtube. The four hodographs in Figure 7 illustrate the ellipticity characteristic of the derived field variations. It is obvious that we obtain ~~from most of the passes~~ well developed ellipses, only when passing close to the center ~~an almost linear relation between $B_{trans}$ and $B_{along}$ results.~~ The artificially looking constant levels of $B_{along}$ are from the passage through the current tube. If we had assumed a more realistic current density distribution that decreases from the center towards the border, the hodographs would have been even more elliptic. In any case, from these four example passes, only the last one, passage close to the center, would have passed our criteria for FAC estimates. This is consistent with our sparse yield of FAC estimates from the longest period band.

So far, we looked only at short data intervals. For obtaining a better impression of the km-scale FACs we have plotted the derived FAC peak densities over the whole study period, 18 September through 4 October 2021. Results from Swarm A and C are again combined. Figure 8 shows the latitude distribution of derived peak current densities from each orbit for the five period bands, covering the period range, 0.1 - 1.2 s (0.4-4.5 km scales). The shortest period band has been dropped because of their fairly small amplitudes, and the two longest periods are not show because of their sparse yield of reliable FAC estimates.

Figure 8 presents in the top row results from the northern hemisphere ~~and in the lower half~~ FAC densities from the southern hemisphere. The left column depicts km-scale FAC activity in the late evening sector around 21:00 MLT, which is the typical local time for substorm onsets. ~~In the~~ right column ~~we~~ show ~~the activity of small~~ FACs ~~around~~ prenoon hours. Because of the large range of derived FAC densities, a logarithmic scale has been chosen for the color bar. From both time sectors and over the whole study period we find clear evidence that largest FAC densities, up to 100 μA/m$^2$ are observed around the period range 0.16-0.26 s (0.6 - 1 km scale size). For longer periods the peak amplitudes significantly ~~drop~~ or fall ~~even~~ below our amplitude threshold.

Commonly, the km-scale FACs occupy only narrow latitude ranges of the auroral region, which vary with local time. In the prenoon sector, right column, this range is found at the poleward border of the auroral oval, around 80° MLat. Only occasionally signals are detected down to 60° MLat. In the southern hemisphere, regularly appearing gaps of current density are observed in the prenoon sector. They are caused by the fact that the Swarm A/C orbits in certain longitude sectors do not reach sufficiently high magnetic latitudes in the southern hemisphere. The extension of FAC activity to lower latitudes is achieved at similar UT times every day in both hemispheres. In the left column of Figure 8, the pre-midnight km-scale FACs appear predominantly around 70° MLat. This is the typical latitude for substorm activity. Also here, on certain days the activity extends to high latitudes. The appearance of FAC activity over a wide latitude range is an orbital effect. On most orbits the Swarm satellites approach the auroral region on their upleg arc around late evening and pass over through midnight to the morning sector. But due to the displacement of the magnetic pole, in some longitude sectors the passage goes from evening via noon sector to the morning side. In those cases, the left column ~~plots~~ contain also some noontime activity at high latitude. Similarly, the right columns contain some orbit-related duskside signal at lower latitude. Generally, in the southern hemisphere the FAC activity is not so well confined in latitude as in the north. This is caused by the larger offset between magnetic and geographic poles in the south. Thus, the MLT and MLat coverage by Swarm is varying much more between orbits in the southern than in the northern hemisphere.

When looking at km-FAC amplitudes, the densities on the dayside vary typically around 10 μA/m$^2$ but occasionally reach up to 100 μA/m$^2$. In the pre-midnight sector the amplitudes are about an order of

https://doi.org/10.5194/egusphere-2025-1961
Preprint. Discussion started: 19 May 2025


magnitude smaller. This confirms earlier results that ~~the large-amplitude very small~~ FACs ~~prefer to~~ appear in the sunlit high latitudes, particularly in the cusp~~,~~ cleft region.

The previously shown results have identified the apparent period range 0.16-0.44 s (0.6-1.7 km scale) as the one where FAC densities peak. Now it would be interesting to see the spectral distribution of FAC density during times of enhanced activity. Figure 9a presents, as an example, a 5-min segment from 30 September 2021 of a pass through the cusp/cleft region in the southern hemisphere, which comprises a rather long passage through a region of intense small scale FAC activity. Shown are the $\Delta B_{trans}$ and $\Delta B_{along}$ components from Swarm A and C. Fluctuations reach up to 2000 nT/s. The interval from 23:41:30 to 23:44:00 UT is used for a harmonic analysis. Resulting spectra from the two components are presented in Figure 9b. Here the spectral amplitudes have been averaged over a half-octave frequency range, in order to enhance the significance of the amplitude curve. Furthermore, the spectral results from Swarm A and C have been combined. A quite obvious spectral feature of both curves is the steep drop in signal strength towards lower frequencies. This is caused by the high-pass filter with a cutoff period at 5 s (Log10(0.2 Hz) = -0.7). The spectra from the two magnetic field component, $\Delta B_{trans}$ and $\Delta B_{along}$, exhibit very similar shapes but the spectral amplitude from $\Delta B_{trans}$ is larger by a factor of about 1.5 than that of $\Delta B_{along}$. This indicates that the FAC sheets are ~~preferably~~ aligned ~~with the~~ magnetic latitude ~~circle.~~

Over the main part of the covered frequency range, we find a rather flat spectrum. Just at the high-frequency end, beyond about 8 Hertz, it starts to roll off. This is consistent with our observation of smaller FAC amplitudes within the shortest period band (0.04-0.1 s, 0.15-0.4 km scale). On the other hand, we find in Figure 6 also FAC amplitude decreases towards the long-period end, a trend which is not reflected by the spectra. Obviously, the spectral shape is governed by the randomly appearing narrow large FAC spikes. They are causing an almost white spectrum reaching far into the lower frequency region. In that way they seem to override the contributions of longer-period signals to the spectrum.

## 6. Discussion

The focus of this study is on the km-scale FACs. However, we have included here also a part of the small-scale FACs with scale sizes of 5 to 20 km. These small-scale FACs were at the center of interest in our recent paper, Lühr and Zhou (2025). By using the high-resolution magnetic field data with a sampling rate of 50 Hz, here we extend the previous study to the smallest FAC scales. Furthermore, the previous investigations already indicated that there might be a connection between the two classes of FAC structure. ~~In spite of that,~~ the two classes exhibit rather different characteristics. The km-scale FACs are made up of randomly ~~appearing large~~ current density spikes. As a consequence, an almost "white spectrum" is obtained from the harmonic analysis of the magnetic field variations (see Fig. 9), reaching far into the longer period range. These spectral features are consistent with the results of Rother et al. (2007) who investigated kilometer-scale FACs based on 5 years of CHAMP data. They also report a flat FAC amplitude spectrum with a high-frequency role-off starting at 8 Hz. They argue that very intense narrow FACs appear randomly and with ~~that cause~~ a spectrum ~~with~~ a long tail towards lower frequencies~~, which~~ overlaps with the signals from the longer-period FAC structures. The upper cut-off frequency is determined by the typical width of the largest spikes~~. This is obviously~~ about 1 km (7.5 [km/s] / 8 [Hz]), as reported by Rother et al. (2007) and found here. The good agreement with their ~~large~~ statistical study suggests that our single spectrum represents ~~the~~ features of the km-scale FACs ~~already quite well~~.

The km-scale FACs are limited to certain latitude regions ~~which depend on~~ local time. Individual features are short-lived, only of order 1 second. When visiting the same location 2 s later, ~~no comparable~~ structure is left. ~~Largest~~ FAC densities ~~are found for~~ horizontal scale sizes of 0.5-2 ~~km~~.

Conversely, ~~our~~ small-scale FACs ~~are~~ found to be stationary over about 18 s. They exhibit a longitudinal correlation length of about 12 km~~,~~ and ~~can be found~~ over wide ranges of auroral latitudes. Whenever the small-scale FACs are accompanied by ~~large~~ km-scale current structures their correlation properties between ~~the~~ recordings at the two Swarm satellites are compromised. This is quite obvious when comparing Figures

https://doi.org/10.5194/egusphere-2025-1961
Preprint. Discussion started: 19 May 2025


3 and 8. The ratio of well-correlated small-scale FACs (2.5-5 s period) in Figure 3 ranges around 90%, except ~~for~~ some latitude bands. ~~Just for these latitude ranges Figure 8 shows intense km-scale FAC activity both on the day and night sides.~~ We regard this effect as a consequence of spectral leakage from the km-scale into the small-scale FAC signal range.

In spite of the listed differences between the characteristics of the FAC classes, there seems to be a ~~strong~~ relation between them. As an example, the magnetic field variations ~~of~~ a northern hemisphere polar pass on 21 September 2021 around 16:55 UT are shown in Figure 10. Presented ~~are~~ in the upper two panels km-scale variations in the period range 0.44-0.72 s and in the four lower panels results from the small-scale range with periods of 2.5-5 s. Bursts of ~~large~~ signal are encountered in both period bands on the nightside and in the morning sector. Note, that the amplitudes of $\Delta B_{trans}$ are about 4 times larger for km-scale signal than for the small-scale FACs. ~~Synchronously~~ with the appearance of ~~large~~ km-scale signal ~~the cross-correlation coefficient, *Cc*, of the small-scale variations drops~~. Reduced *Cc* values at other locations, not accompanied by km-scale features, are caused by the very low signal amplitude of the small-scale signal. ~~There are~~ two other features~~, worth to be mentioned.~~ The km-scale variations only appear in connection with small-scale signal, and small-scale FACs reach largest amplitudes only in regions where also km-scale signal appear. ~~Already~~ Lühr and Zhou (2025) ~~stated~~ that ~~preferably~~ large-amplitude small-scale FACs ~~suffer~~ reduced cross-correlation ~~coefficients caused by the~~ ~~even stronger~~ amplified km-scale signals. These latter findings strongly suggest a connection between the ~~synchronous~~ appearance of amplified small- and km-scale FACs.

For ~~the~~ explanation of that connection, we should have a closer look into the characteristic of the small-scale FACs. For example, Park et al. (2017) made use of Swarm electric field and magnetic field data to determine the reflection properties of the ionosphere for Alfvén waves~~. Interestingly, they selected the apparent~~ period range from 2 to 15 s ~~for their investigations.~~ This range overlaps very well with our class of small-scale FACs as defined in Lühr and Zhou (2025). Due to limitations of the E-field instrument on Swarm, Park et al. (2017) could not ~~cover~~ all seasons and local times ~~too well~~, but for equinox conditions in 2014 they ~~get~~ a fairly complete picture. ~~This fits well our~~ September, October 2021 dataset considered here. ~~Those authors derive among others~~ the wave reflection coefficient, α. The value α = 0 indicates a complete ~~dissipation~~ of the wave in the ionosphere, hence no reflection. Conversely, α = 1 is expected for a perfectly conducting ionosphere which ~~will cause~~ a total wave reflection. From the relation between E- and B-field ~~variations~~ they ~~could~~ confirm that the variations within their selected period range act like Alfvén waves. Park et al. (2017) report largest reflection coefficients around 75° MLat on the sunlit dayside and around 65° MLat on the dark nightside with values of α = 0.3 - 0.5. This ~~means, a good part of the incident wave is reflected~~ in the region where we observe the small-scale FAC bursts.

It is well established that Alfvén waves can oscillate between the ionosphere and a magnetospheric reflection layer~~, forming the~~ ionospheric Alfvén resonator (e.g. Lysak, 1991). More recent studies show~~ed~~ that Alfvén wave packets ~~when running into each other from different sides will~~ generate~~, by interaction,~~ wave components ~~of~~ shorter wavelengths and higher frequencies (e.g. Maron and Goldreich, 2001; Chandran, 2004). When ~~this process of wave package bouncing back and forth is going on~~ for a sufficiently long time, ~~accompanied by many package collisions,~~ the magnetic field ~~variations will turn into~~ turbulent ~~fluctuations~~. We suggest that ~~such a kind of~~ process ~~is going on~~ in the latitude region ~~of our~~ bursty signals. We think that the Alfvén waves, carrying our small-scale FACs, suffer repeatedly collisions of oppositely travelling waves and by that transfer more and more signals into shorter wavelengths and higher frequencies. This process requires, however, continuous input of ~~new~~ wave energy ~~that the~~ losses ~~by~~ dissipation ~~when bouncing at the ionosphere are compensated.~~ It probably even needs an increasing rate of power input from the magnetosphere and a long-lasting source of waves for generating the brought spectrum of the large amplitude small-scale FACs and the huge narrow spikes of km-scale FACs, as observed by Swarm, e.g. in the cusp region. Park et al. (2017) ~~report~~ reflection coefficients of α = 0.3 - 0.5 for ~~their~~ small-scale Alfvén waves. ~~That means, at least half of the energy gets lost on each reflection. However, for km-size transverse scales~~ Pilipenko et al. (2002) estimate higher reflection coefficients of order α = 0.9. These values are

https://doi.org/10.5194/egusphere-2025-1961
Preprint. Discussion started: 19 May 2025


consistent with our observations that km-scale FACs gain more in amplitude than the small-scale FACs inside the activity bursts. However, these authors also state that Alfvén waves below a certain spatial size are strongly damped upon traversing the ionosphere. The km-scale structures also seem to exhibit higher harmonic frequencies (>0.5 Hz) in the Alfvén wave resonator. This can explain the observed decorrelation between signals that are sampled only 2 s apart.

A remaining question is, what determines the smallest FAC sizes. The quasi-white spectrum starts to roll-off at an apparent frequency around 8 Hz. The corresponding 1 km can be regarded as the smallest wavelength of these bursty FACs. In a ~~dedicated~~ model study Lotko and Zhang (2018) have investigated the ionospheric dissipation properties of short-wavelengths ~~Alfvénic structures.~~ As expected, for longer wavelength (>20 km) they find largest Joule heating rates in the E-region. For shorter wavelengths and in particular, for higher harmonics ~~resonating Alfvén waves the~~ dissipation in the F-region becomes increasingly important. ~~This process~~ limits ~~the growth rate of too small structures.~~ The resulting ~~effect of~~ heating at F-region altitudes, predicted by their model, is well supported by the observations of local air upwelling in connection with km-scale FACs in the cusp region (e.g. Lühr et al., 2004). In addition, these authors point out that single-satellite recordings of small Alfvénic structures suffer from ~~the wavelength/frequency~~ ambiguity when flying through regions ~~of these~~ very small ~~current structures.~~ Thus, determining ~~the actual~~ properties ~~of~~ the smallest scales is ~~not easy~~ from ~~our~~ Swarm observations. ~~Besides that,~~ Lotko and Zhang (2018) ~~claim~~ that absorption ~~of dispersive waves with~~ wavelengths < 0.5 km, ~~in~~ the F-region~~,~~ occurs at altitudes above 2,000 km. ~~This absorption is due to wave-particle interactions with electrons, and it~~ produces the soft (broadband) electron precipitation that ~~is~~ commonly accompanying bursts of km-scale FACs (e.g. Watermann et al., 2009). ~~All these statements~~ provide a convincing explanation for our observations that largest current densities are achieved by km-scale FACs.

## 7. Summary and conclusion

In this study we investigated the characteristics of the smallest-scale field-aligned currents at auroral latitudes. For this purpose, we used the high-resolution magnetic field data ~~from~~ the closely spaced Swarm A and C spacecraft ~~sampled at 50 Hz~~. Particularly suitable are the 16 days ~~around~~ the quasi-coplanar ~~constellation~~ 1 October 2021, as part of the counter rotating orbit phase. During those days the along-track separation between the spacecraft was reduced to 2 s and the cross-track separation varied only between 0-3 km. This special ~~constellation~~ enabled ~~us to derive several unknown characteristics of~~ km-scale and small-scale FAC structures at auroral latitudes. Major results of the study are listed below.

1. For small-scale FACs (5-20 km sizes) the stability features reported by Lühr and Zhou (2025) ~~could be~~ confirmed. However, due to the very limited range of temporal and spatial separations~~,~~ ~~experienced~~ during the 16 days of this study, ~~no~~ upper limit could be determined. By applying the ellipticity analysis to the magnetic signals, caused by this type of FACs, we found that the currents are organized preferably in filaments rather than current sheets.

2. The km-scale FACs (0.5-5 km size) exhibit markedly different characteristics. Narrow FAC spikes ~~with large amplitudes~~ appear quasi randomly. ~~No indication of stability could be determined between quasi collocated measurements separated by only 2 s.~~ This confirms the very transient character of these km-scale FACs. ~~Largest~~ FAC densities, exceeding ~~partly~~ 100 μA/m$^2$, ~~are observed for~~ horizontal scales of 0.5-2 km. Peak amplitudes rapidly decrease towards shorter and longer scales.

3. The appearance of km-scale FACs is ~~commonly~~ confined to narrow latitude ranges of about 5°. These latitude ~~bands are depending on~~ local time. Within the noon and prenoon sectors FAC activity is predominately ~~found~~ around 80° MLat, while on the nightside and dusk sector, it ~~appears~~ more ~~frequently~~ around 70° MLat. ~~On the dayside large~~ FAC densities, ~~typically~~ between 10 and 100 μA/m$^2$, are observed. ~~Differently, on the nightside the~~ amplitudes ~~are commonly smaller by~~ an order of magnitude.

https://doi.org/10.5194/egusphere-2025-1961
Preprint. Discussion started: 19 May 2025


4. The magnetic field variations from the km-scale FACs, recorded by Swarm, exhibit an almost white frequency spectrum. ~~Towards higher frequencies~~ a spectral roll-off starts at 8 Hz. This corresponds to an along-track wavelength of about 1 km. The low-frequency end of the flat spectrum ~~exceeds well our~~ band limit of 0.2 Hz, ~~thus cannot be quoted here.~~ This observation confirms earlier suggestions that spectral leakage from the km-scale signal into the period range of small-scale FACs contaminates the magnetic signature of ~~these latter current structure. As a consequence of that,~~ the degree of cross-correlation between Swarm A and Swarm C recording is reduced for small-scale FACs ~~whenever~~ km-scale FAC ~~appear~~.

5. In spite of the ~~clearly~~ different characters of small- and km-scale FACs, they seem to be closely connected. ~~For example,~~ small-scale FACs reach largest amplitudes when km-scale currents appear. ~~Furthermore,~~ km-scale FACs are always accompanied by small-scale FACs. Based on these facts we suggest that small-scale FACs are part of the generation process for the narrow large FAC spikes. In our view, e.g. patchy reconnection launches Alfvén waves of 5-50 km horizontal size at F-region altitude. These waves are partly reflected at the ionosphere, travelling back up again. Meanwhile, reconnection has launched more Alfvén waves, which will run into the reflected. By interaction of these oppositely propagating waves, smaller scales and higher harmonic resonances will be generated. When this process goes on for a sufficiently long time quasi-chaotic field variations will result. Smallest scales are determined by the enhanced ionospheric damping of those small structures.

After having elucidated important characteristics of the km-scale FACs, it would be interesting to see for example, their effect on thermospheric heating and/or thermospheric winds. Also, of interest would be to see the electric field accompanying such small structures, and are there particular particle populations appearing together with these narrow FACs? The Swarm satellites are not suitable to provide answers to these questions, but others may do.

## Data Availability Statement

The authors thank the European Space Agency for openly providing the Swarm data. The data products used in this study are Level-1b MAGx_HR with version number 0605, which are available at the European Space Agency website: https://earth.esa.int/web/guest/swarm/data-access.

## Author contributions

YLZ performed the data collection, analysis, editing. HL contributed to the concept and the first draft of the manuscript. Both authors finalized the manuscript.

## Competing interests

The authors declare that none of the authors has any competing interests.

## Acknowledgements

The work of Yun-Liang Zhou is supported by the National Nature Science Foundation of China (42174186).

https://doi.org/10.5194/egusphere-2025-1961
Preprint. Discussion started: 19 May 2025


## References

Anderson, B.J., H. Korth, C.L. Waters, D.L. Green, V.G. Merkin, R.J. Barnes, and L.P. Dyrud (2014), Development of large-scale Birkeland currents determined from the active magnetosphere and planetary electrodynamics experiment. Geophysical Research Letters 41: 3017–3025. https://doi.org/10.1002/2014GL059941

Chandran, B.D.G. (2004), A review of the theory of incompressible MHD turbulence, Astrophysics and Space Science 292: 17–28.

Finlay, C. C., Kloss, C., Olsen, N., Hammer, M., Toeffner-Clausen, L., Grayver, A., & Kuvshinov, A. (2020). The CHAOS-7 geomagnetic field model and observed changes in the South Atlantic Anomaly. Earth Planets and Space, 72(1), 156. https://doi.org/10.1186/s40623-020-01252-9

Fowler, R. A., B. J. Kotick, and R. D. Elliott (1967), Polarization analysis of natural and artificially induced geomagnetic micropulsations, J. Geophys. Res., 72, 2871.

Friis-Christensen, E., H. Lühr, D. Knudsen, and R. Haagmans (2008), Swarm—An Earth observation mission investigating Geospace, Adv. Space Res., 41, 210–216, doi:10.1016/j.asr.2006.10.008.

Iijima, T. and Potemra, T. (1976), Field-aligned currents in the dayside cusp observed by Triad, J. Geophys. Res., 81, 5971–5979.

Lotko, W., & Zhang, B. (2018). Alfvénic heating in the cusp ionosphere-thermosphere. Journal of Geophysical Research: Space Physics, 123, 10,368–10,383. https://doi.org/10.1029/2018JA025990

Lühr, H., M. Rother, W. Köhler, P. Ritter, L. Grunwaldt (2004), Thermospheric up-welling in the cusp region, evidence from CHAMP observations, *Geophys. Res. Lett.,* **31,** L06805, doi:10.1029/2003GL019314.

Lühr, H., P. Ritter, G. Kervalishvili and J. Rauberg (2020), Applying the Dual-Spacecraft Approach to the Swarm Constellation for Deriving Radial Current Density, in *Ionospheric Multi-Spacecraft Analysis Tools*, M. W. Dunlop and H. Lühr (eds.), (ISSI Scientific Report Series; 17), 117-140, Springer Nature Switzerland.

Lühr, H., and Y.-L. Zhou (2025), Small- and meso-scale field-aligned auroral current structures, their spatial and temporal characteristics deduced by Swarm constellation, Annales Geophysicae, 43, https://angeo.copernicus.org/preprints/angeo-2024-28/.

Lysak, R. L. (1991), Feedback instability of the ionospheric resonant cavity, J. Geophys. Res., 96, 1553–1568, doi:10.1029/90JA02154.

Maron, J. & P. Goldreich (2001), Simulations of incompressible magnetohydrodynamic turbulence, The Astrophysical Journal, 554:1175-1196.

Neubert, T. and Christiansen, F. (2003), Small-scale, field-aligned currents at the top-side ionosphere, Geophys. Res. Lett., 30, 2010, doi:10.1029/2003GL017808.

Park, J., H. Lühr, D. J. Knudsen, J. K. Burchill, and Y.-S. Kwak (2017), Alfvén waves in the auroral region, their Poynting flux, and reflection coefficient as estimated from Swarm observations, J. Geophys. Res. Space Physics, 122, 2345–2360, doi:10.1002/2016JA023527.

Pilipenko, V. A., Fedorov, E. N., and Engebretson, M. J.: Alfvén resonator in the topside ionosphere beneath the auroral acceleration region, J. Geophys. Res., 107, 1257, doi:10.1029/2002JA009282, 2002.

Ritter, P., H. Lühr, and J. Rauberg (2013), Determining field-aligned currents with the Swarm constellation mission, Earth Planets Space, 65(11), 1285–1294, doi:10.5047/eps.2013.09.006.

https://doi.org/10.5194/egusphere-2025-1961
Preprint. Discussion started: 19 May 2025


624 Rother, M., Schlegel, K., & Lühr, H. (2007). CHAMP observation of intense kilometre-scale field-aligned
625 currents, evidence for an ionospheric Alfvén resonator. Annales Geophysicae, 25, 1603-1615.
626 doi:10.5194/angeo-25-1603-2007.

627 Watermann, J., Stauning, P., Lühr, H., Newell, P. T., Christiansen, F., and Schlegel, K. (2009), Are small-
628 scale field-aligned currents and magnetosheath-like particle precipitation signatures of the same low-
629 altitude cusp?, Adv. Space Res., 43, 41–46, doi:10.1016/j.asr.2008.03.031.

630 Xiong C. & Lühr H. (2023). Field-aligned scale length of depleted structures associated with post-sunset
631 equatorial plasma bubbles. *J. Space Weather Space Clim.* 13, 3.
632 https://doi.org/10.1051/swsc/2023002

633 Zhou, Y.-L., Lühr, H., & Rauberg, J. (2024). Horizontal scales of small- and meso-scale field-aligned
634 current structures at middle and low latitudes. Journal of Geophysical Research: Space Physics, 129,
635 e2024JA032857. https://doi.org/10.1029/2024JA032857

636

637

https://doi.org/10.5194/egusphere-2025-1961
Preprint. Discussion started: 19 May 2025


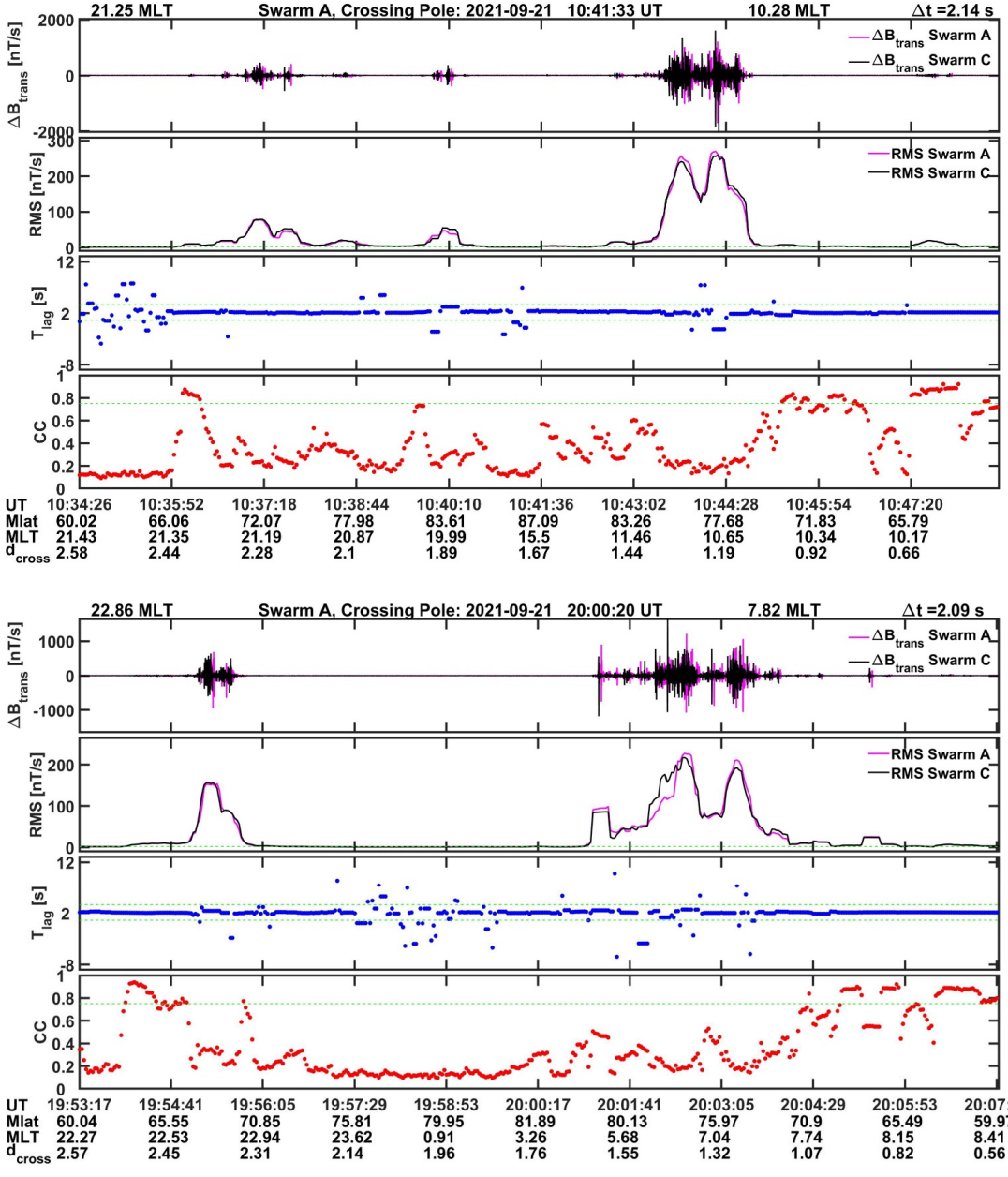


**Figure 1.** Examples of magnetic variations in the transverse, $\Delta B_{trans}$, component within the period range of 0.04 - 5 s. The top panels of the two frames show the recordings of Swarm A and C along their orbits, crossing the polar region of the northern hemisphere. The second panels reflect the RMS value of the signal amplitude. The third panel contains the lag time, T-lag, between the signals for which the peak cross-correlation is achieved. The correlation coefficient, *Cc*, derived between Swarm A and C signal is shown in the bottom panels. For most of the values low correlation coefficients, $Cc < 0.75$, are found. The dashed green lines mark the thresholds for the stability criteria. Along the horizontal axis temporal and spatial information is provided. The $d_{cross}$ lists the spacecraft separation in cross-track direction.

https://doi.org/10.5194/egusphere-2025-1961
Preprint. Discussion started: 19 May 2025


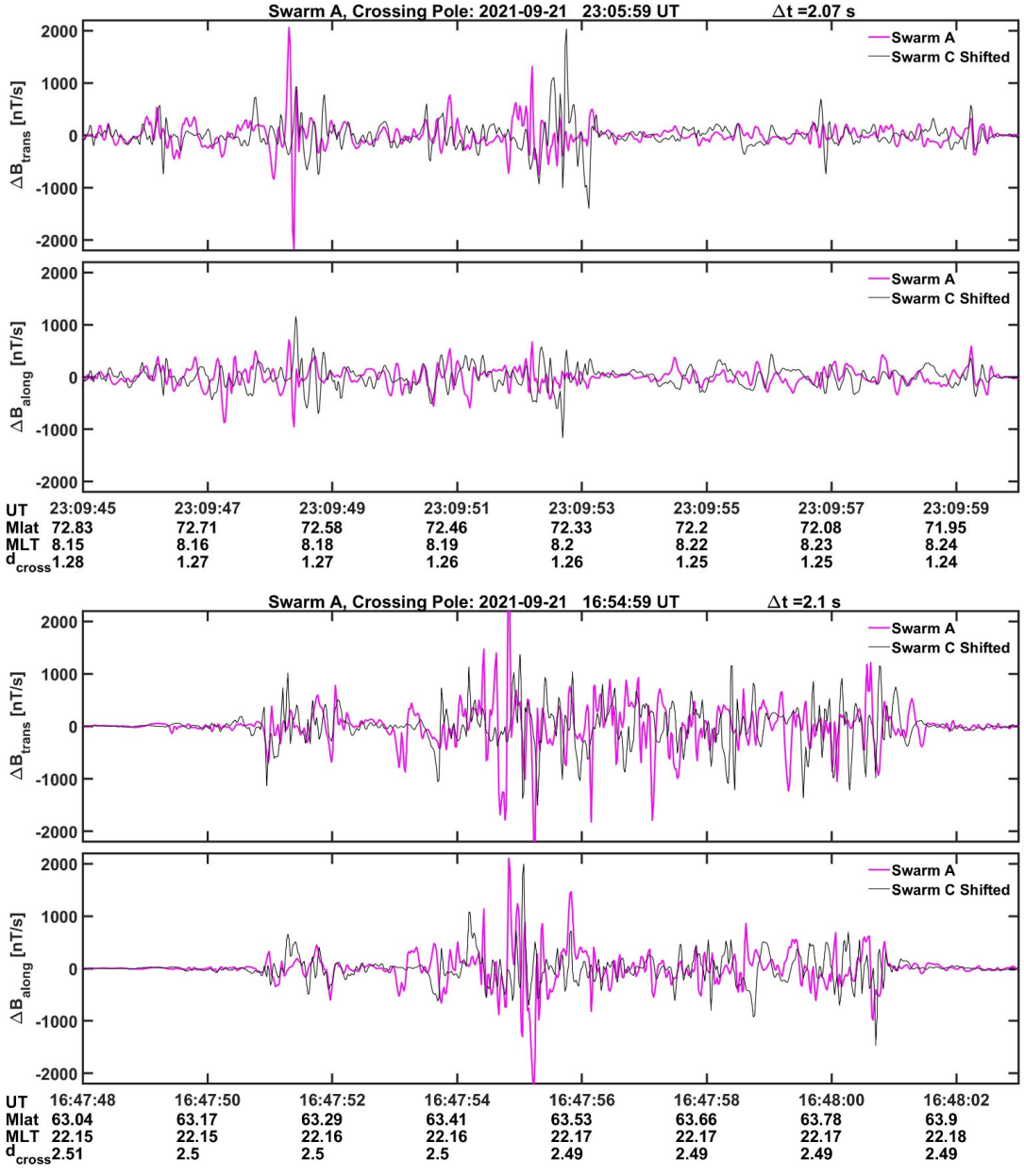


**Figure 2.** Examples of $\Delta B_{trans}$ and $\Delta B_{along}$ variations during bursts of km-scale FACs from the prenoon sector in the upper frame and from the nightside in the lower frame. Largest amplitudes are confined to very small scales. There is hardly any correlation observed between Swam A and C recordings.

https://doi.org/10.5194/egusphere-2025-1961
Preprint. Discussion started: 19 May 2025


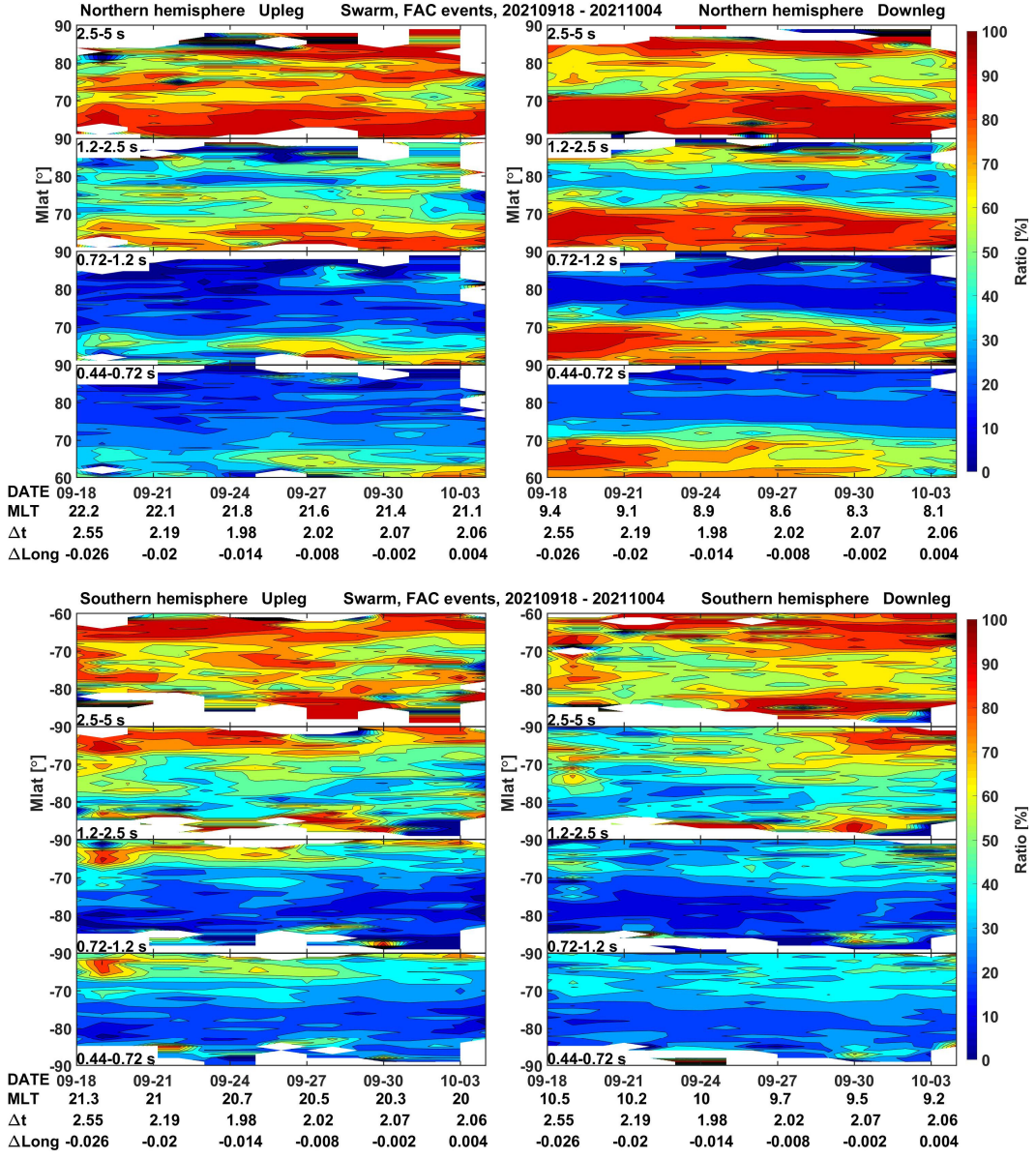


**Figure 3.** Latitude distribution of the ratio between positively detected stationary FAC structures and all wavy signals with amplitudes above the threshold of RMS > 2 nT/s, separately for four period bands. Separate frames present up- and downleg orbital arcs, and the two hemispheres. The labels along the horizontal axis include the along-track time difference, Δt, and the longitudinal difference at equator crossing between the spacecraft, ΔLong, in degree.

https://doi.org/10.5194/egusphere-2025-1961
Preprint. Discussion started: 19 May 2025


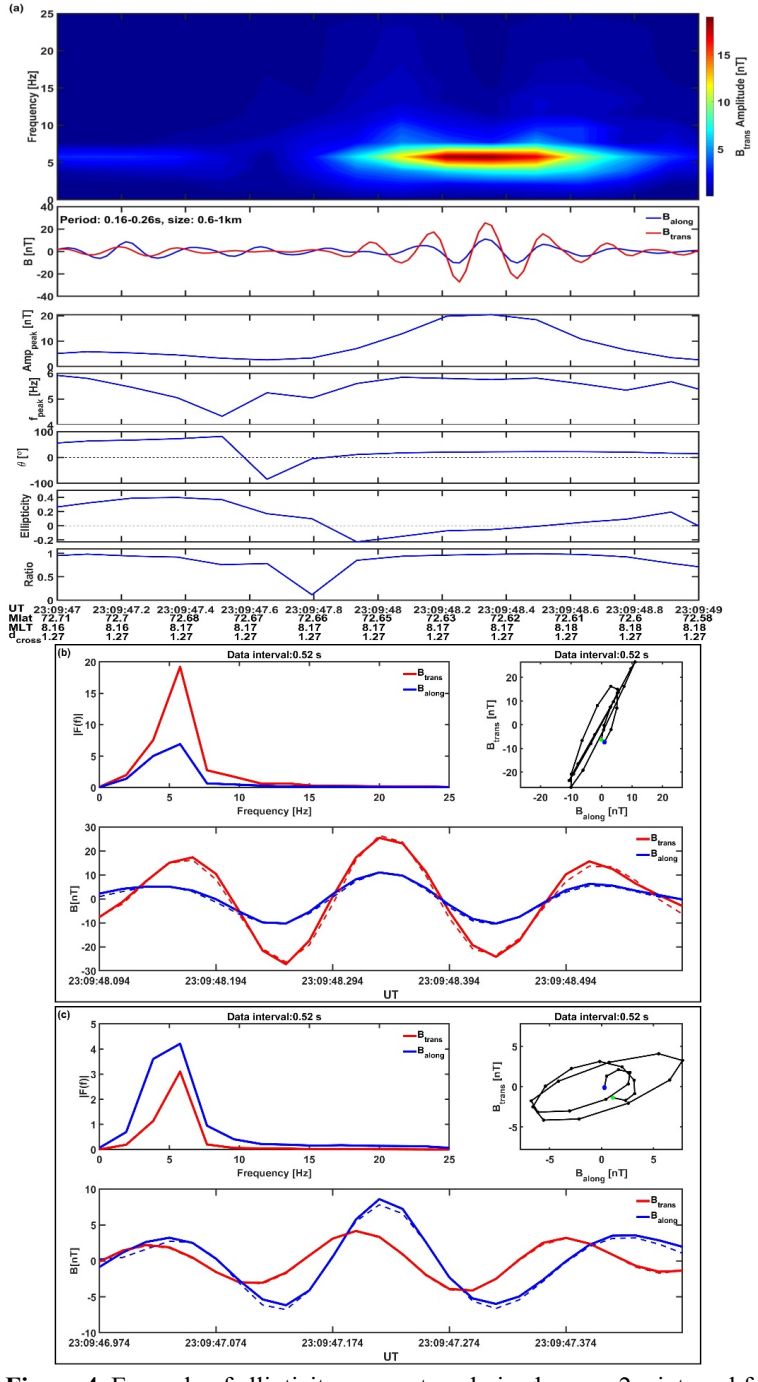


**Figure 4.** Example of ellipticity parameters derived over a 2-s interval for the 0.16-0.26 s period band. (a) the top panel displays the dynamic spectrum of the magnetic signal, below the time-lines of the two field components are shown. The five lower panels outline the temporal variations of the parameters determined by ellipticity analysis. (b) and (c) details of the magnetic signals for two processing intervals.

https://doi.org/10.5194/egusphere-2025-1961
Preprint. Discussion started: 19 May 2025


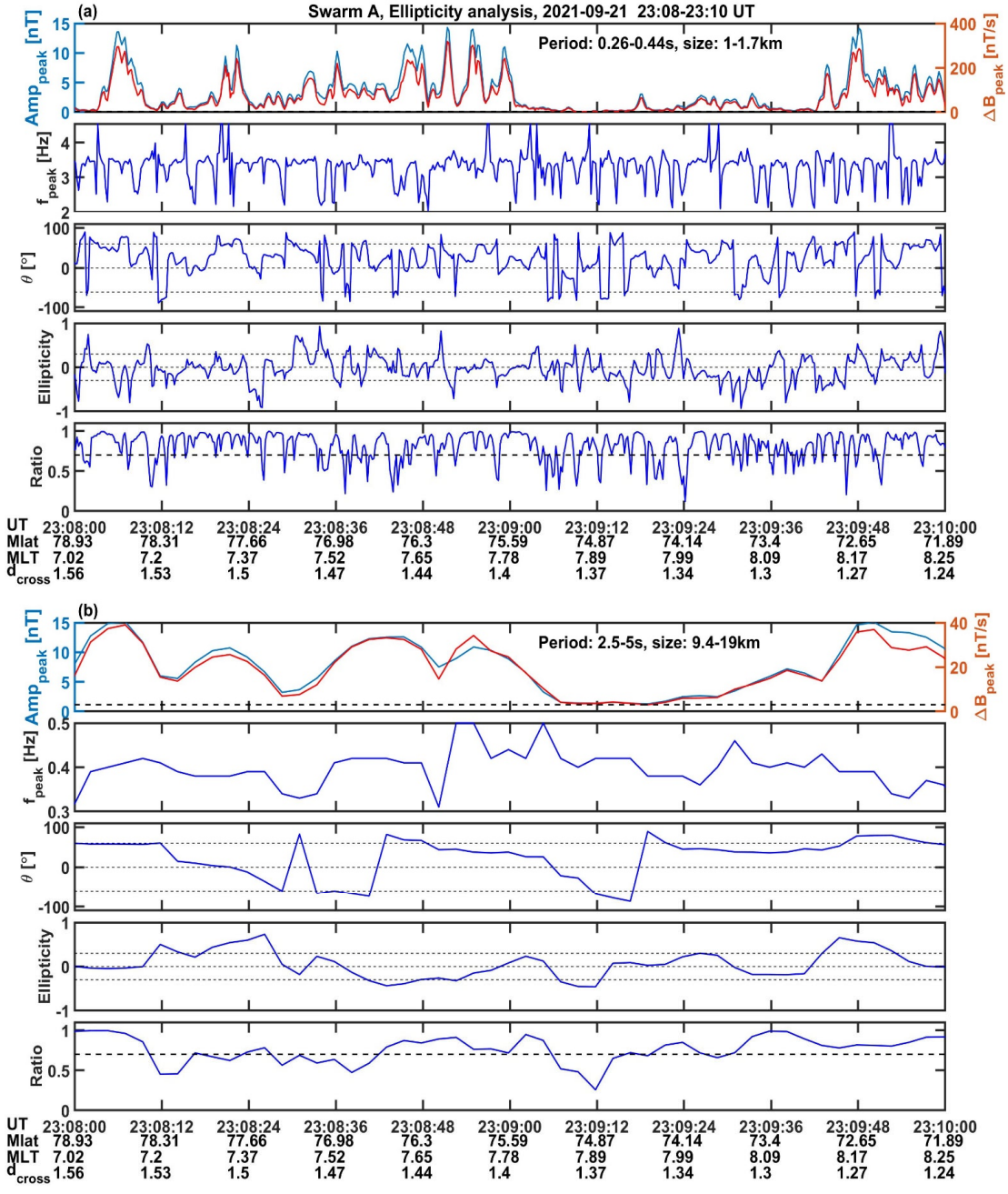


**Figure 5.** Temporal variation of the ellipticity parameters for a 2-min time interval. Dashed lines mark the thresholds that are considered for the estimation of reliable FAC densities. (a) Ellipticity parameters for the 0.26-0.44 s period band, (b) The same for the 2.5-5 s period band.

https://doi.org/10.5194/egusphere-2025-1961
Preprint. Discussion started: 19 May 2025


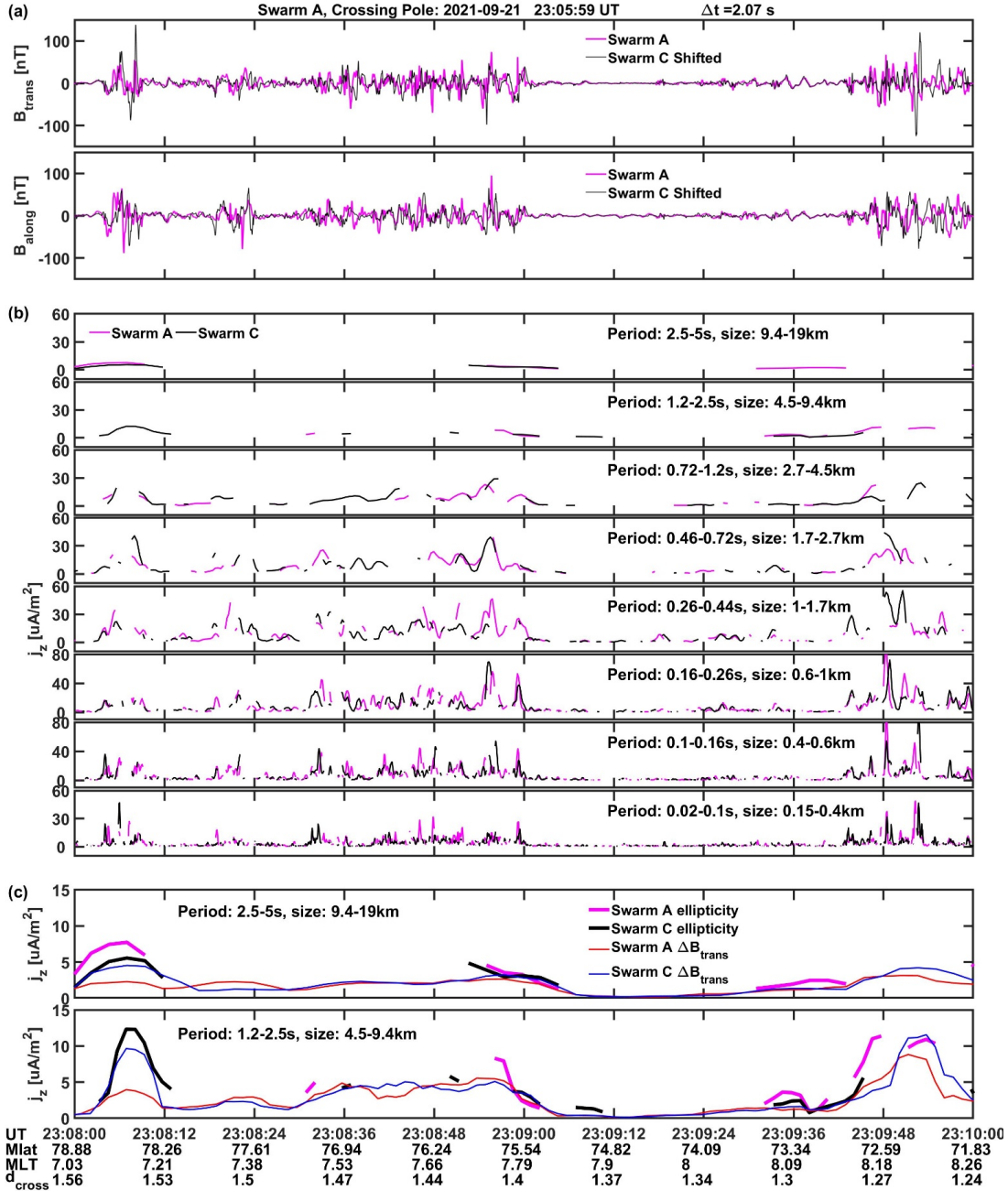


**Figure 6.** Temporal variation of FAC density estimates over a 2-min interval. (a) Timelines of $B_{trans}$ and $B_{along}$ variations over the considered interval, as recorded by Swarm A and C. (b) FAC density estimates derived from the ellipticity parameters, separately for all 8 period bands. (c) Comparison of FAC densities estimated by the simple single-satellite technique (thin lines) with results from the ellipticity approach (heavy line segments), for the two longest period bands.

https://doi.org/10.5194/egusphere-2025-1961
Preprint. Discussion started: 19 May 2025


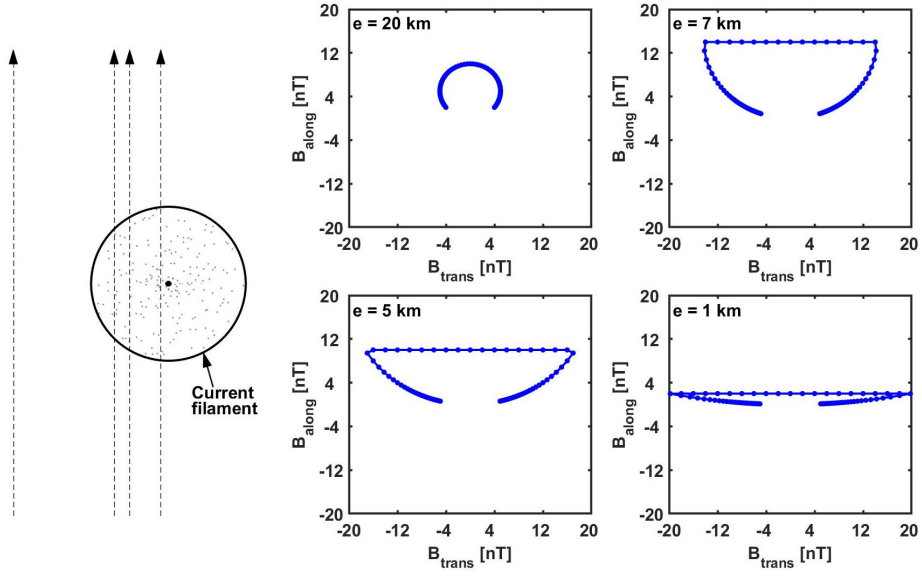


**Figure 7.** Modelling of the magnetic field ellipticity signatures for passes by a circular current tube of 10 km radius. On the left side the considered 4 trajectories past the current tube are illustrated. Resulting hodographs of the expected field variations are for all the tracks. Constant values of the $B_{along}$ components come from measurements inside the tube with a homogeneous current density distribution.

https://doi.org/10.5194/egusphere-2025-1961
Preprint. Discussion started: 19 May 2025


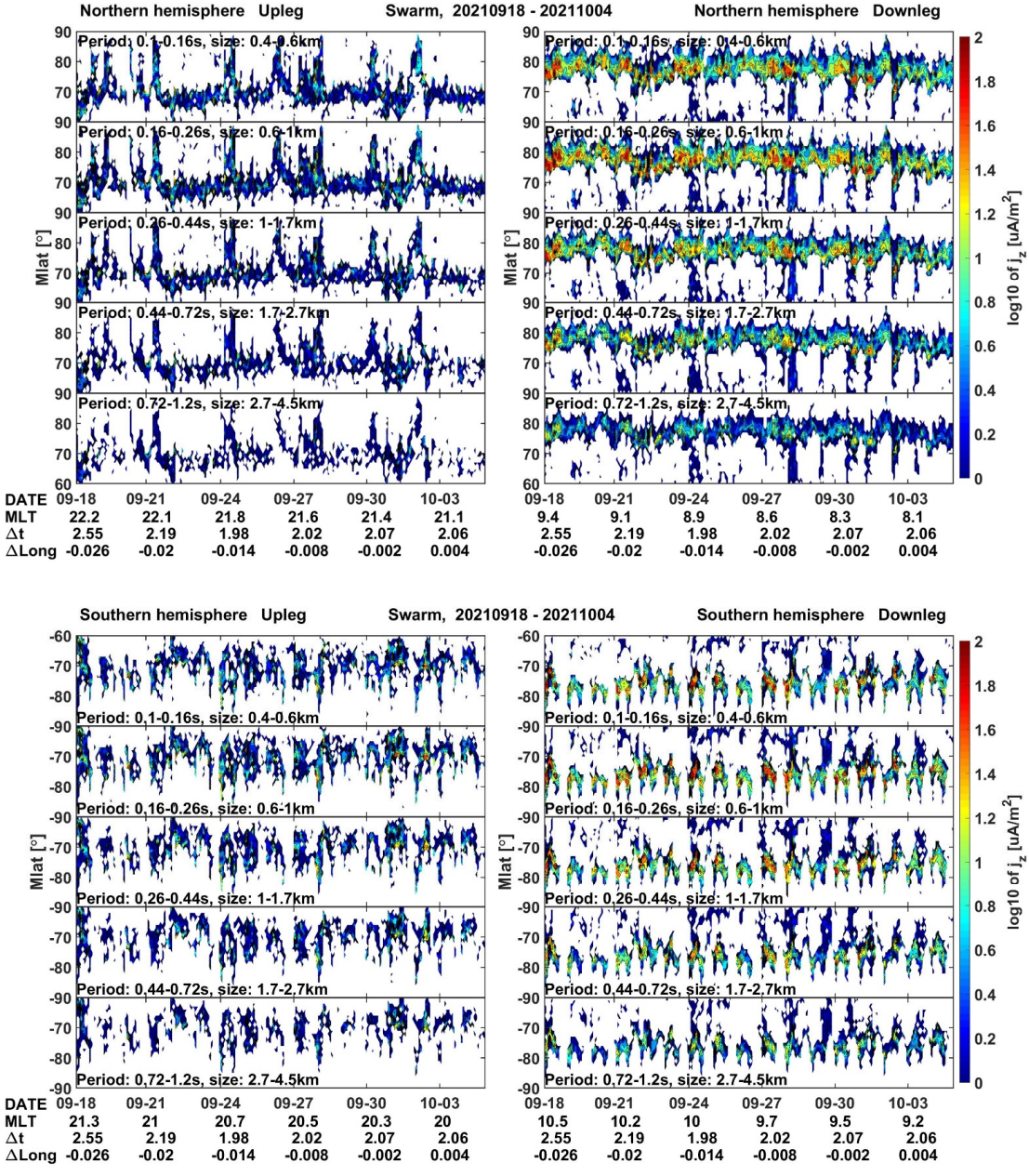


**Figure 8.** Latitudinal distribution of km-scale FAC density for the five period bands with largest amplitudes. The format is the same as that of Figure 3, but only structures of horizontal scale sizes of 0.4-4.5 km are shown. White areas mark ranges without entries.

https://doi.org/10.5194/egusphere-2025-1961
Preprint. Discussion started: 19 May 2025


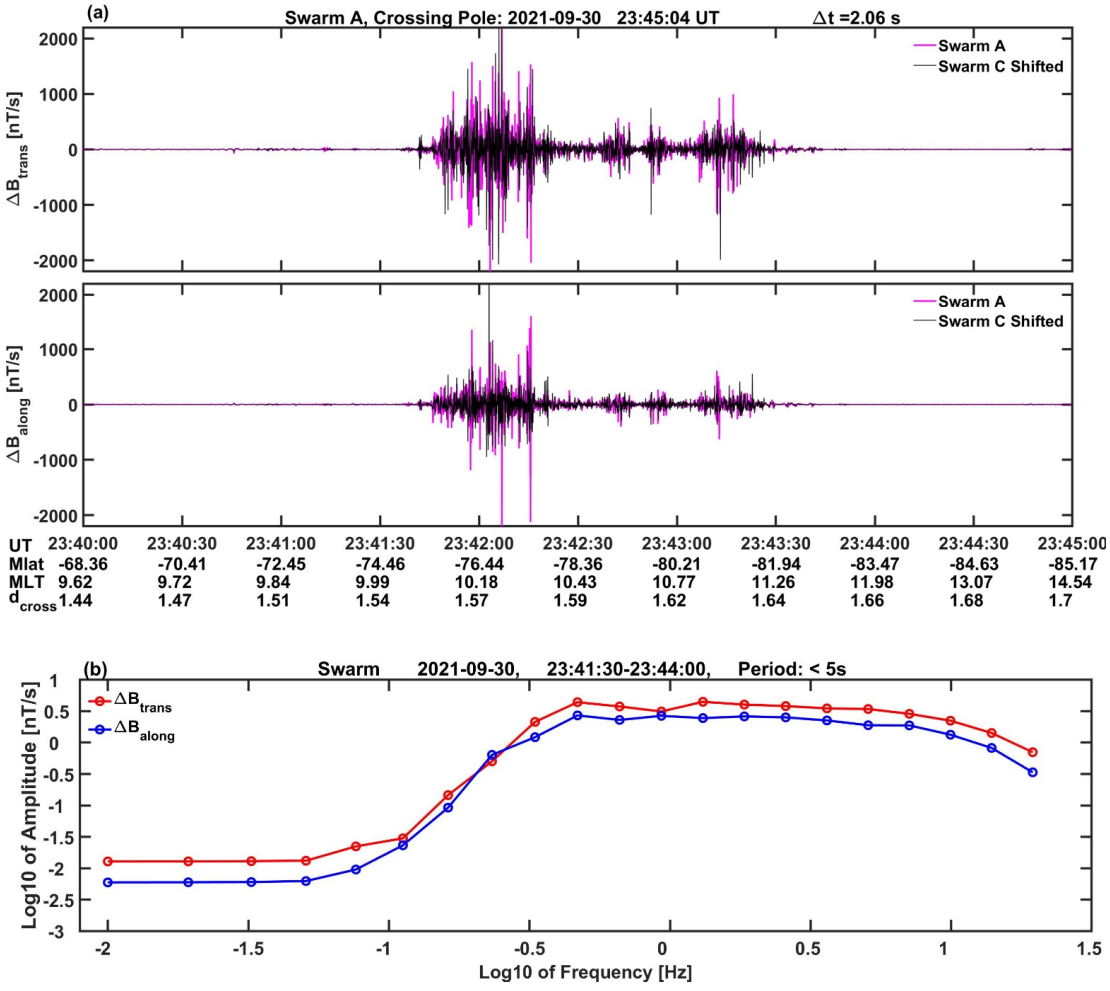


**Figure 9.** Example of signal spectra for a typical burst of km-scale FAC activity, separately for the field components $\Delta B_{trans}$ and $\Delta B_{along}$. The steep amplitude roll-off around 0.2 Hz is caused by the applied high-pass filter.

https://doi.org/10.5194/egusphere-2025-1961
Preprint. Discussion started: 19 May 2025


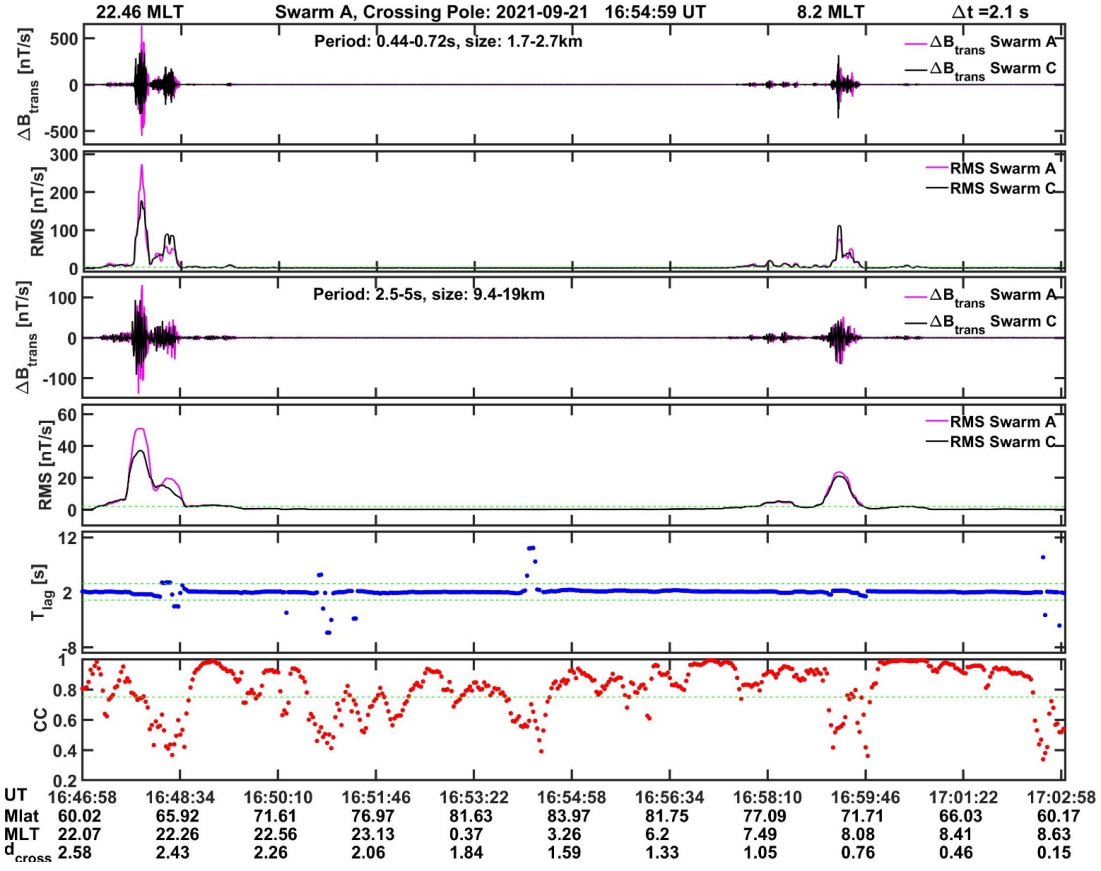


**Figure 10.** Comparison of magnetic field variation ($\Delta B_{trans}$ component) between the km-scale and small-scale FAC classes. Activity enhancements appear simultaneously, but at the same times the cross-correlation coefficient of small-scale current structures goes down. The format is the same as Figure 1.